

Model Validation of Loose Bolted Joints in Damaged Structural Systems

Joel R. Feenstra¹, Tyler F. Winter², Brandon R. Dierschke³, Alan Barhorst⁴

¹Dept. of Mechanical Eng., Michigan Technological University, Houghton, MI 49931

²Dept. of Mechanical and Aerospace Eng., University of Missouri-Rolla, Rolla, MO 65401

³Dept. of Mechanical Eng., Texas A&M University, College Station, TX 77843

⁴Dept. of Mechanical Eng., Texas Tech University, Lubbock, TX 79409-1021

NOMENCLATURE

I	Area Moment of Inertia
E	Modulus of Elasticity
m	Total Mass
L	Length
η	Efficiency of Impact
U	Eigenvectors or Mode Shapes
M	Mass Matrix
C	Damping Matrix
K	Stiffness Matrix
f_n	Natural Frequency
W_n	Model Natural Frequency Matrix

ABSTRACT

The bolted or riveted lap joint is a common fastening technology for structural members. When a joint becomes worn the joined members can move in a nonlinear fashion relative to each other as well as impact each other and the lap joint plates. For low frequency bending modes the system can experience sticking or frictional sliding motion at the finite number of contact points in the joint. This research validates a low order theoretical frictional contact impact model of a typical loose bolted joint. For each of the different contact and motion regimes damping parameters were determined. Contact patches, strain gauges, a force transducer, and accelerometers were used to measure the response of a test device. The results were then compared to the simulation results. A video of the experimental joint motion was also compared to animations of the simulated joint. The simulation parameters were adjusted to produce a better prediction of the behavior of the test device.

1 INTRODUCTION

The bolted lap joint is a very common connection method for structural members. The joints do not form a perfect connection and they can be a major source of structural damping. When the joints wear, they can exhibit complex nonlinear behavior including impact. A low order (9 degrees of freedom) model was developed by

Barhorst [1-4] to simulate a single bolted joint structure. Figures 1 and 2 show a schematic view of how the structure is setup in the model. There is a coordinate system for each of the six bodies with generalized coordinates, q , for the rigid motion and distributed coordinates \tilde{u} for the elastic motion.

To validate the model, the experimental test setup shown in Figure 3 was used to collect strain, input force, and acceleration, as well as record the contact events between the end beam and the joint plates at four locations as depicted in Figure 4. These data were then compared to the computer simulation results. The simulation parameters were then adjusted to produce a better match. An important part of the validation was the identification of the simulation parameters. The damping characteristics for the different joint motion regimes were the first parameters investigated. The mass, inertia, geometry, and material properties were also determined.

This paper will proceed with the motivation for the work followed by background research of the state-of-the-art. After that, the approach to modeling, parameter identification and how the experiment was setup will be discussed in more detail. Lastly the results from previous work and this work will be discussed.

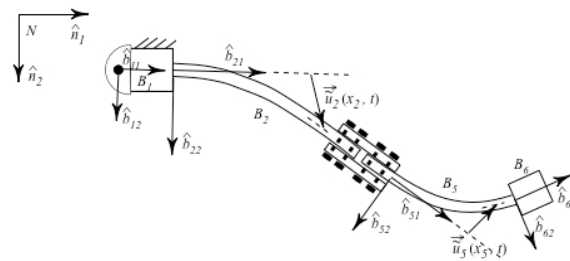


Figure 1 – Beam and Joint Diagram

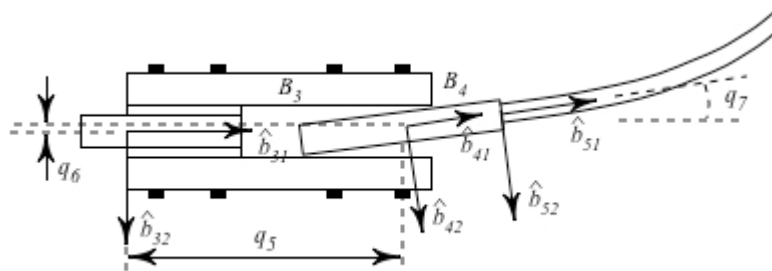


Figure 2 – Rigid Joint Diagram

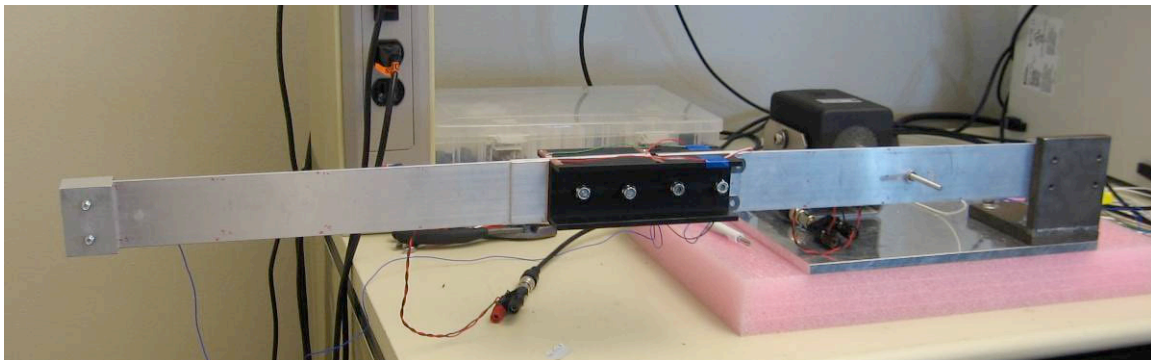


Figure 3 – Test Setup

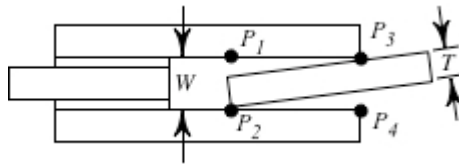


Figure 4 – Joint Contact Points

2 MOTIVATION

Bolted joints are used in many different applications. Buildings, aircraft, robots, and many other structures use bolted joints in some form or another. The ability to model the behavior of the joint over its entire lifespan would be useful in extending service life. In addition, a model that can handle impact type nonlinearities provides utility to future experiments. Having a low order model that can accurately simulate the joint would also provide a low-cost way to help monitor and mitigate damage in a joint. Where the mitigation might be implemented via model based control. Another application is structural health monitoring, where this model type might be used as a basis for a damage parameter estimator for clearance type nonlinear damage.

3 BACKGROUND RESEARCH SUMMARY

Much attention has been paid over the past few years to the study of different joint types, including the bolted lap joint. Most of the work has been in the area of microslip and macroslip phenomenon [6, 7]. Microslip occurs when small parts of the joint interface slip and usually occurs under low joint excitation. When the excitation increases, the entire interface can slip, which is called macroslip.

Research performed at Sandia National Laboratories [5, 6] showed there is a power law relationship between excitation and the energy loss (damping) of the joint. They used an experimental setup to validate an Iwan model [11, 12] of the joint that could describe the damping and stiffness characteristics of both the microslip and the macroslip effects [6]. An Iwan model uses a series of blocks connected with springs and dampers to model the joint interface.

Pratt and Pardoen [7] used a 7000 DOF finite element model to study the behavior of a bolted lap joint common in airplanes. Their results were within 5% of the experimental results. They only studied tight joints. The higher order model they used would not be practical for situations involving many joints due to the cost of running a finite element model of this type. Gaul and Lenz [14] also use a finite element model to simulate the stick/slip properties of a bolted joint.

Moloney, Peairs and Roldan [8] used a low-order finite element model that used a bristle model of friction. Results showed an accurate match to the experimental results once the bristle model was modified to include a direct dependency on velocity. They concluded that the damping of a lap jointed beam is an increasing function of amplitude.

Most of the available research assumes that the joint is in good condition and tight. Barhorst [1-4] proposes a significantly different model. The biggest change is that the joint is initially loose. This causes complex nonlinearities such as impact. It also means that there are a number of different motion regimes that must be modeled. The approach to rigid and flexible body dynamics that Barhorst follows is developed elsewhere [9, 10].

4 MODELING METHOD

The model developed by Barhorst [1-4] simulates the extreme wear of the joint shown in Figures 1 and 2. It is a low order (9 DOF) model that uses a hybrid-parameter multiple-body system (HPMBS) modeling methodology that is based on the variational approach of Gibbs-Appell. Figures 1 and 2 show how the coordinate systems for the 6 bodies are laid out. Body 1 is a fixed body that exists because the model was originally designed for use in a slewing beam. The second body and the fifth body are modeled as flexible beams. Hermite polynomial approximations are used as their shape functions [1]. All of the other bodies are modeled as rigid.

Figure 3 shows how the contacts inside the joint are designated. There are a total of seventeen different motion regimes. The regime can be sticking or slipping in single point contact at four different contact locations (points 1-4 in Figure 3). It can also be sticking or slipping at any of four different two-point contact modes which are labeled: 1-3, 1-4, 2-3 and 2-4. For example, 1-3 indicates contact at points 1 and 3, 2-4 means contact at 2 and 4, etc... The last motion regime corresponds to the end beam in free-flight and is labeled 0 for purposes of plotting. The switching from one regime to another is handled using instantly applied nonholonomic constraints to reduce the degrees of freedom [1]. Momentum is then transferred based on individual algebraic transfer equations (a total of 54 equations are needed). This method does not require coefficients of restitution or penalty methods to handle the contact constraints because there are enough field equations to determine the momentum transfer.

The momentum transfer sets the initial conditions for the new motion regime. The integrator, Livermore solver for ordinary differential equations (LSODA), evolves the states of the system until the motion regime changes and the process is repeated. This continues until the final time is reached, see Barhorst [1-4] for modeling and simulation development details.

5 PARAMETER IDENTIFICATION

There are a large number of parameters that must be identified before execution of the simulation. These include masses, inertias, dimensions, locations of the measurement devices, input force level and frequency, energy loss due to impact, joint gap width, and various damping parameters. Results from the previous work [15] suggested that the damping parameters needed to be properly identified.

In order to determine the damping parameters, modal tests were performed on the inner and outer beams and the whole structure. Modal tests were performed for the outer beam with five different boundary conditions: free-free, single point sticking contact at point 1 or 2, single point sticking contact at 3 or 4, and two point contact (both sticking and slipping). The data was then analyzed for mode shapes, frequencies, and damping using MEScope™. Table 1 summarizes the results from these tests.

Table 1 – Damping Estimates

1st Beam Damping Estimates		2nd Beam Damping Estimates	
Configuration	Average ζ	Contact Regime	Average ζ
No Joint, No Stinger	0.0287	Free	0.0045
No Joint, With Stinger	0.0667	2 Sticking	0.0355
With Joint, No Stinger	0.0040	2 Slipping	0.0346
		12 Sticking	0.0088
		34 Sticking	0.0036

The damping matrices were derived from the modal tests and were transformed into the coordinate system used in the model. To do this the mode shapes from the linearized model were used as a transformation for the diagonal modal damping matrix. The resulting matrix was then pre-multiplied by the mass matrix and the diagonal terms were taken to be the state damping terms in the simulation as shown:

$$W_n = \sqrt{U^{-1}(M^{-1}K)U}$$

and

$$C_{model} = M U (2\zeta_{modal} W_n) U^{-1} \tag{1}$$

Another important term was the energy loss due to impact. This number ranged from 0 to 1 and adjusted how much velocity was removed from the states right after impact. This number produced widely varying results and was one of the parameters that were varied in order to produce the best results. It should be noted that this is not a coefficient of restitution because no assumption of body separation is made. These terms try to model the energy loss to sound generation and other un-modeled dynamics. The percent change in kinetic energy was measured using the efficiency of energy loss due to impact (η) as shown:

$$\% \Delta KE = (\eta^2 - 1) 100 \quad (2)$$

The mass and inertia properties were determined by weighing the parts and creating solid models to find the inertia of the more complex pieces (joint and stiffeners). The locations of the accelerometers and the strain gauges were measured as well as the lengths of all of the bodies and subsequently input into the simulation.

There was an attempt to determine the elastic modulus of the beams using an accelerometer on a cantilevered beam where first mode harmonic bending was assumed. The natural frequency (f_n), mass (m), area inertia (I), and length of the beam were used to determine Young's modulus as shown:

$$E = \left(\frac{2 \cdot \pi \cdot f_n}{3.52} \right)^2 \frac{m \cdot L^3}{I} \quad (3)$$

This did not produce believable results ($E = \sim 48 \text{ GPa}$). A couple of other approaches were tried and rejected. In the end the nominal published value was used.

6 SIMULATION

The simulation [4] is a FORTRAN program that runs in Cygwin under Windows. It uses a text file for input with all of the previously mentioned parameters. To improve the model a large number of parameter variations were tested. Typically the gap width, energy loss, and damping parameters were varied. Damping parameters were varied from the measured modal values, discussed above, based on the peaks and valleys in the experimental data. Once a damping parameter was chosen, the simulation was executed and the results were compared to the experiment. If improvement was necessary the energy loss from impacts was adjusted and the simulation rerun. The process was repeated until the best results for the given damping parameters were obtained. New damping parameters were then picked until suitable results were obtained. In addition to damping and energy loss the whole process was repeated for different gap widths and input frequencies and amplitudes.

7 EXPERIMENT

7.1 TEST APPARATUS

The test apparatus used in the experiment consisted of two aluminum beams and a joint made from two plastic C-channels. The first beam was cantilevered from a steel and aluminum base at one end and bolted to two aluminum plates and the C-channels at the free end. The second beam was bolted to the C-channel and two more aluminum plates and the free end of the second beam had a removable mass attached to it. A shaker was fixed to the base and connected to the first beam at a point 13 cm from the fixed end of the beam. Figure 5 depicts the entire apparatus fully assembled. The dimensions of the beams and the C-channels are provided in Table 2.

Table 2 - Dimensions of the Major Parts of the Apparatus

	Length (cm)	Height (cm)	Width (cm)
Beam 1	36.5	5.0	0.3
C-Channel	15.5	2.5	0.5
Beam 2	44.0	5.0	0.3

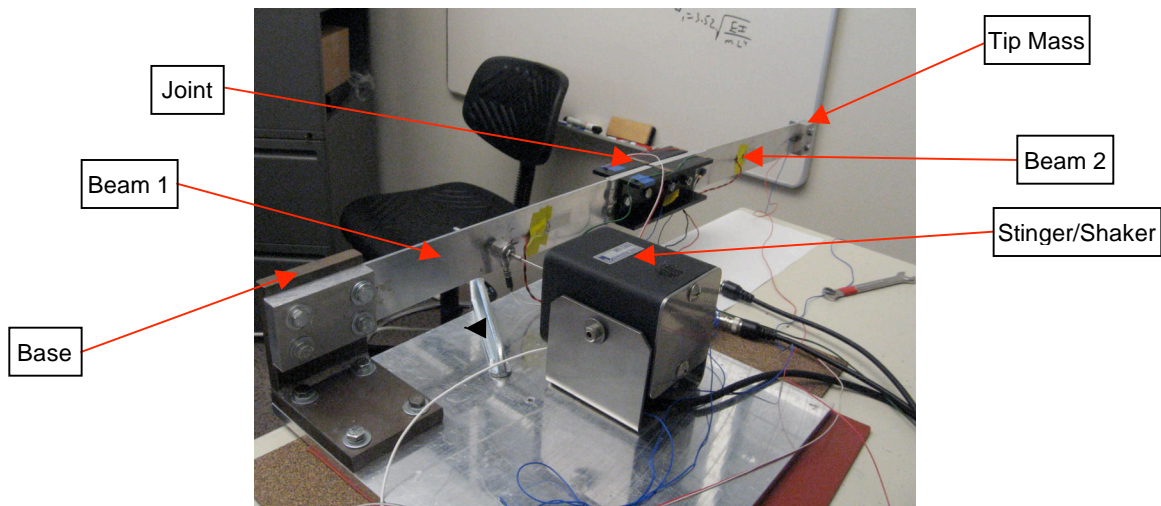


Figure 5 - Fully Assembled Test Apparatus

The aluminum plates were used to stiffen the sections of the beams where they are attached to ensure rigidity in the joint which was assumed in the model [1-4]. The joint was made of C-channels to further ensure stiffness in the joint. A plastic material was used for the joint because it needed to be non-conductive for implementation of the contact sensors. Feeler gauges were inserted between the plates and the joint on the side connected to the first beam to simulate damage. This extra space caused the second beam to be loose and move partially independent from the first beam.

7.2 SENSORS

Six different sensors were used to assess the response of the system. One force transducer was placed on the stinger connecting the shaker and the first beam. One strain gauge was attached near the center of each of the two beams. Three accelerometers were attached to the three sections of the apparatus. The name, type, and location of each sensor (from the fixed end of beam one) are shown in Table 3.

Table 3 - Sensor Names, Types and Locations (from base)

Name	Type	Location (cm)
Accel 1	Accelerometer	41.5
Accel 2	Accelerometer	48.5
Accel 3	Accelerometer	77.5
Force	Force Transducer	13
Strain 1	Strain Gauge	22
Strain 2	Strain Gauge	62.5

7.3 CONTACT DETECTION

One response which was difficult to measure was the contact between the loose (second) beam and the joint. The solution to this problem was to use thin copper strips attached to the inside of the joint and a simple circuit to measure a voltage drop when contact is made. A simple schematic of the circuit is shown in Figure 6.

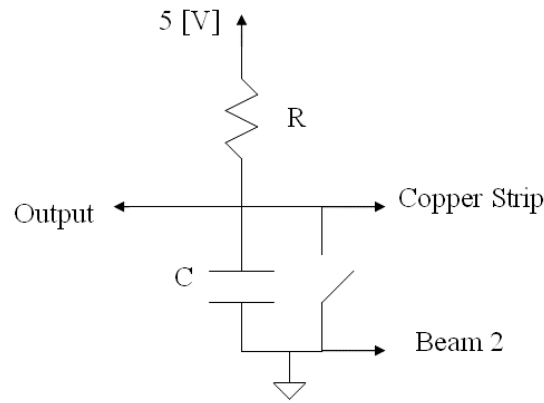


Figure 6 - Schematic for Measuring Contact

The input voltage was kept constant by a regulated power supply, the loose beam was connected to ground and the voltage of each of the copper strips was measured. When the beam was not in contact with the copper, the voltage reading would be greater than zero and when contact was made the reading goes to zero because the copper was grounded. To turn these voltages into discrete on/off data a threshold of 0.1 V was used in Matlab™ while analyzing the data. The resistor was used to keep the amperage to a minimum and the capacitor was used to de-bounce the electrical effects in the circuit. The values of resistance and capacitance were chosen so that the time constant of the circuit was short enough to yield acceptable data.

7.4 EXCITATION

The test apparatus was excited using a Labworks Inc. model ET-132 electrodynamic shaker. The excitation signal was generated in, and output from, a PXI-1042Q from National Instruments and amplified by a Labworks™ linear power amplifier model pa-138. During the experiment two types of signals were used to excite the apparatus. The first excitation was a sine wave with a constant amplitude and frequency output for ten seconds. The duration was long enough to observe the transients die out and the response to become quasi-periodic. The second excitation was a sine chirp from a low frequency (~5 Hz) to a high frequency (~60 Hz) at constant amplitude for a duration of four minutes.

7.5 DATA ACQUISITION

Data was collected using ten inputs on three cards in a PXI-1042Q. The sampling frequency for the ten second sine wave excitation was 10 kHz and for the four minute sine chirp the sampling frequency was 1250 Hz. After each test, the data were written to a text file. Numerical analysis software, Matlab™, was used to open these files and examine the results.

8 PREVIOUS EXPERIMENTAL RESULTS

The results collected during experimental testing in previous work [15] show a need for improved parameters for the model. A visual comparison analysis between experimental and simulation results indicated various aspects of the results. The key differences in previous work [15] were that the joint was secured using an L-channel and contact was measured using four pressure patches. The L-channel seemed to reduce the quality of the experimental results compared to the simulation because the model assumes a rigid joint. The asymmetry of the channel allowed for unwanted flexing that was not modeled in the numerical simulation. There were also problems with measuring contact using the piezo-based pressure patches. One issue was that of handling the thresholds of the patches in determining what constitutes contact. Another issue was that the pressure patches only measure transitions between contacts which were difficult to analyze. The final issue that needed to be addressed was the proper damping values being used for the model. A new way to determine the appropriate damping values was necessary for improving comparison results. For these reasons, additional experimental testing and numerical simulation was vital.

9 CURRENT EXPERIMENTAL OBSERVATIONS

While working with the experiment several observations were noted. First, increasing the gap width caused the nonlinearities to be more pronounced. Second, increasing the amplitude of the forcing function increased the nonlinearities. Third, contact at point three in the joint was lower than expected.

The gap width had a direct effect on the amount of nonlinearities seen in the results. Increasing the gap width allowed for more freedom of the second beam. When the gap width was smaller, the second beam acted as if there was little or no damage. This observation could be seen in the frequency domain. Figure 7 and Figure 8 show the power spectrum of the fast-Fourier transforms (FFTs) of the data collected from Accel3, at the tip of the outer beam, with two different gap widths. The driving frequency is 20 Hz.

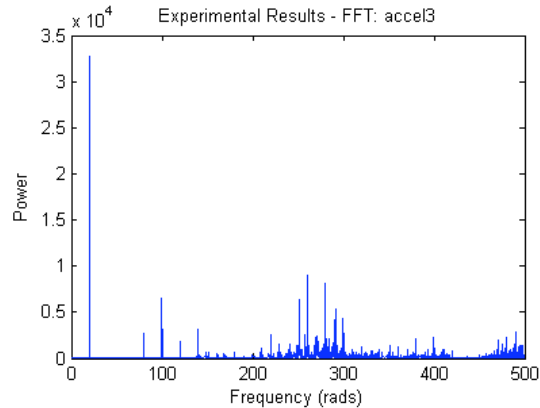


Figure 7 - 0.864 mm Gap Width

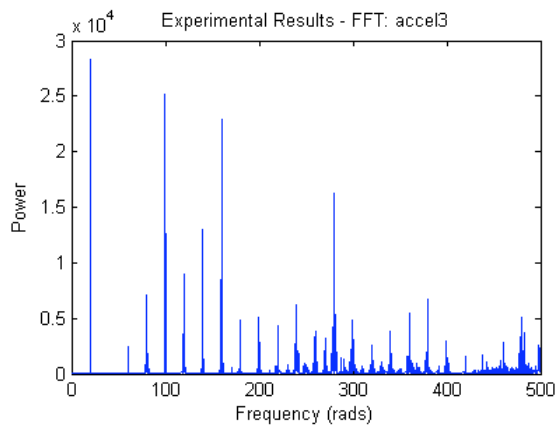


Figure 8 - 1.168 mm Gap Width

Figure 7 shows data from the smallest gap width used and Figure 8 shows data from the largest gap width used. More harmonics are seen in Figure 8 compared to Figure 7 which indicates more contact activity in the joint.

Other observations include that the amplitude of the forcing function caused a change in the nonlinear response of the system. At low amplitudes the sliding friction from the bolts connecting the joint to the loose beam caused the system to behave in a linear fashion. At high amplitudes there was enough force to break the loose beam free and it behaved in a nonlinear fashion.

Contact at point three was observed to be less than expected. The reason for this is unknown but it is thought to be caused by an irregularity on the bolt or in the bolt hole of the loose beam. The hole and bolt were both sanded and lubricated but this did not help the problem much. The only way to get consistent contact was to increase the amplitude.

9 RESULTS

Experimental testing and numerical simulation results were analyzed using four different techniques. The first method was visual inspection of time-domain data. For each of the sensors mentioned above, as well as the contact detection, time history results were collected from the experimental tests and numerical simulations.

Figure 9 shows a comparison with two percent damping on all the states of the model. Figure 10 shows a similar comparison of the time history data for a 20 Hz sinusoid with adjusted damping of roughly 0.1% and a gap width of 0.0864 cm. One can obviously see that with the 0.1% damping, shown in Figure 10, the simulation amplitudes of the time history are significantly better than the simulation amplitudes with two percent damping. The location of the third accelerometer may be coincident with a node, that was observed visually, which would explain the lack of energy detected by the accelerometer. The bands in the time history data seem to be wider since the simulation does not predict the node at the same location as the third accelerometer.

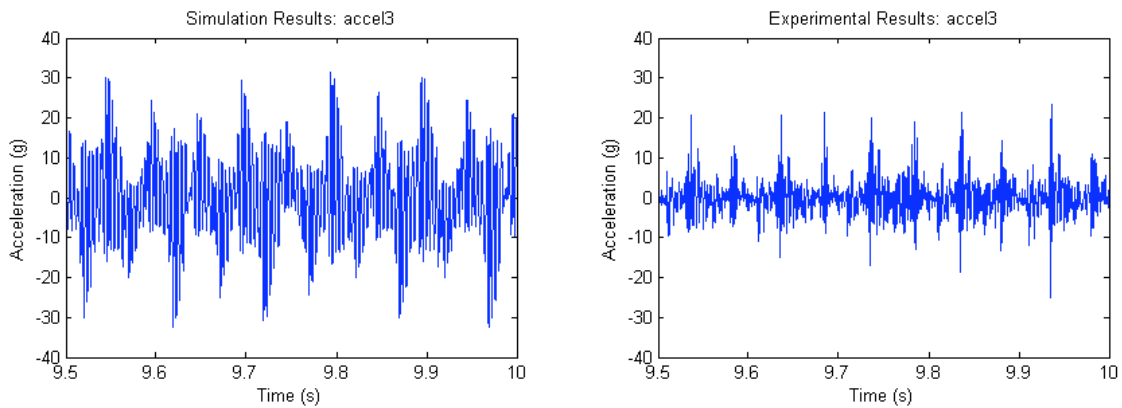


Figure 9 – Time History Data for a 20 Hz Sinusoid (2% State Damping)

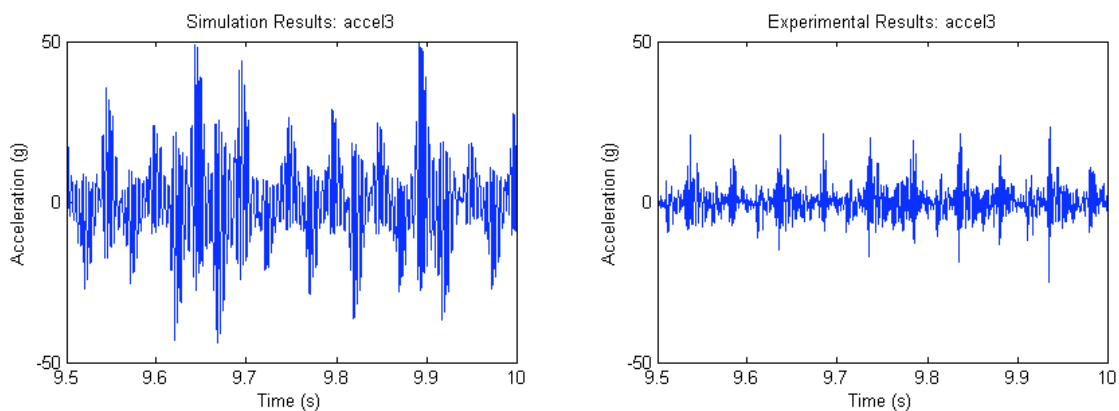


Figure 10 – Time History Data for a 20 Hz Sinusoid (0.1% Damping)

As indicated in Figures 9 and 10, visual inspection of the time-domain results, by itself, provides somewhat of a challenge for analysis. For this reason, the frequency data was examined. Next, an FFT of the time-domain data was calculated and the resulting frequency spectrum was analyzed. By inspecting Figure 11, one can see how

the simulation over predicted the amplitudes at respective frequencies. There also seems to be a great deal of aperiodicity in the simulation results whereas the experimental results show discrete peaks. Figure 12 shows an improvement from Figure 11 in the sense that the peaks are well defined. This improvement is a result of adjusting the damping parameters. Like the time data, the frequency data shown in the simulation may be over predicting the amplitudes because the simulation does not predict a node at that location. The node location predicted by the simulation is further inboard. In Figure 12 it is clear the simulation may be predicting quarter and half harmonics and their multiples as well as the higher harmonics. Overall the results look promising. The burst indicated in the figures are slightly shifted from each other, which is probably caused by the stiffness or mass parameter mismatches.

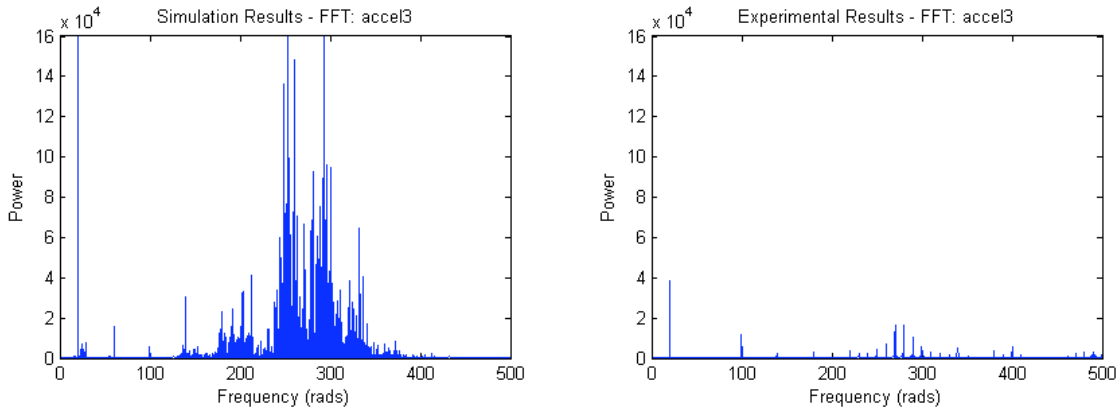


Figure 11 – FFT of Time Data shown in Figure 9

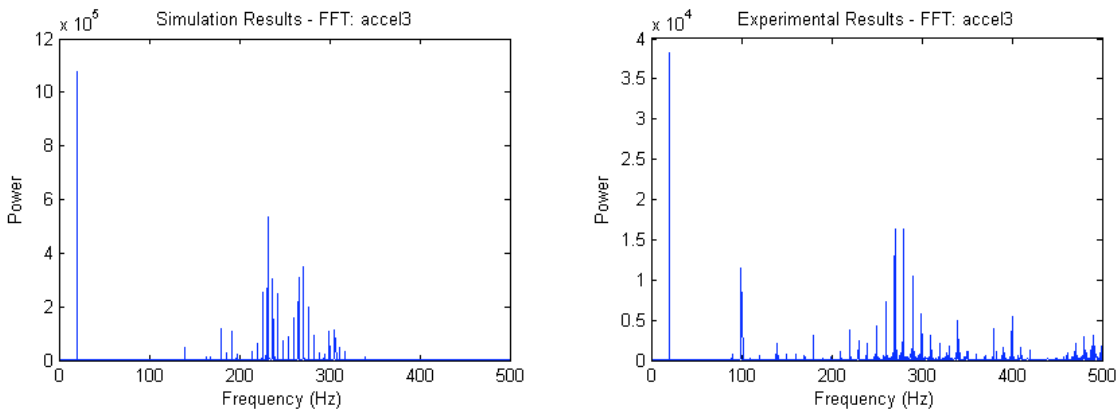


Figure 12 – FFT of Time Data shown in Figure 10

In Figure 13, the strain gauge time and frequency data are displayed. In the figure, the blue highlighted data is the window used for the spectrum calculation. As can be seen from the figure, the strain data amplitude from the simulation is off by a factor of two. The PVDF patches used for strain measurement were calibrated via harmonic response of the individual beams, but there may still be some error. The frequency content of the strain data shows good correspondence between the actual and simulation data, and this is encouraging and supports the model validity. The amplitudes are not an exact match. This could be due to miss-estimation of the damping as well. The factor of two mismatch could be an effect of under-prediction but also may be caused by miscalibration of the data acquisition system from end-to-end.

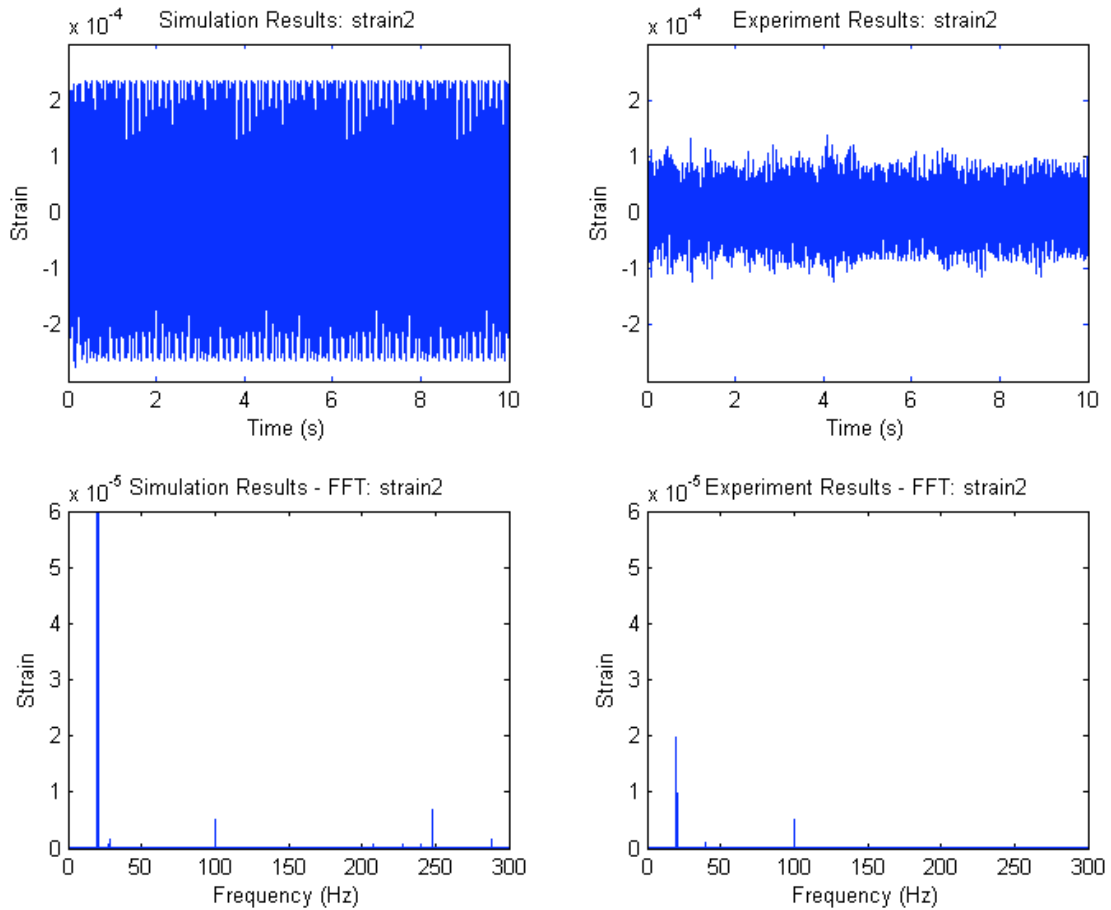


Figure 13 –Time History (top plots) and FFT (bottom plots) Data

Third, the contact histories were examined. Figure 14 shows the time histories and histograms for contact points for the simulation (left) and the experimental tests (right) for Figure 9. Figure 15 shows the same information corresponding to data of Figure 10. The vertical axis in the top two plots in Figure 14 designate the points that were in contact. For example, contact at points one and four would correspond to “14” and no contact corresponds to “0.” After observing Figure 4, one can determine that there are only nine possible contact regimes. For this reason, data will only appear at nine values for contact points in Figures 14 and 15. By viewing Figures 14 and 15, one can see that the contact histories match reasonably well. Both figures show that the beam is switching from contact at points one and four to contact at points two and three, however, the experiment shows more contact at points one and three. To increase correspondence between the figures, the simulation would need to predict the beam in the “free” regime more often and less contact at points 1-4.

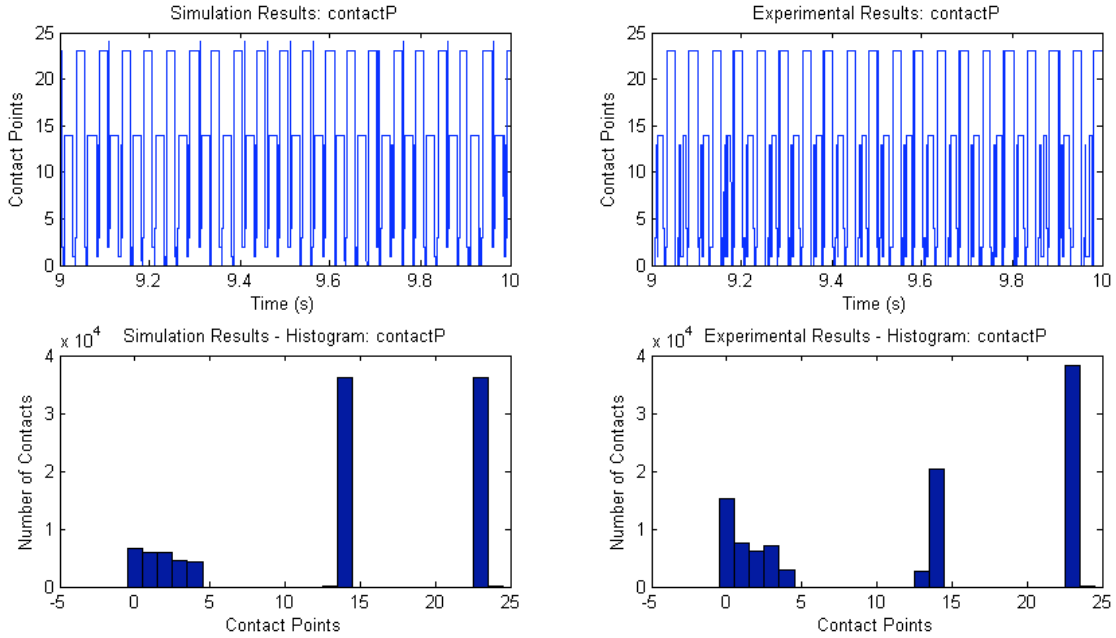


Figure 14 – Contact Time Histories and Histograms Results for Figure 9

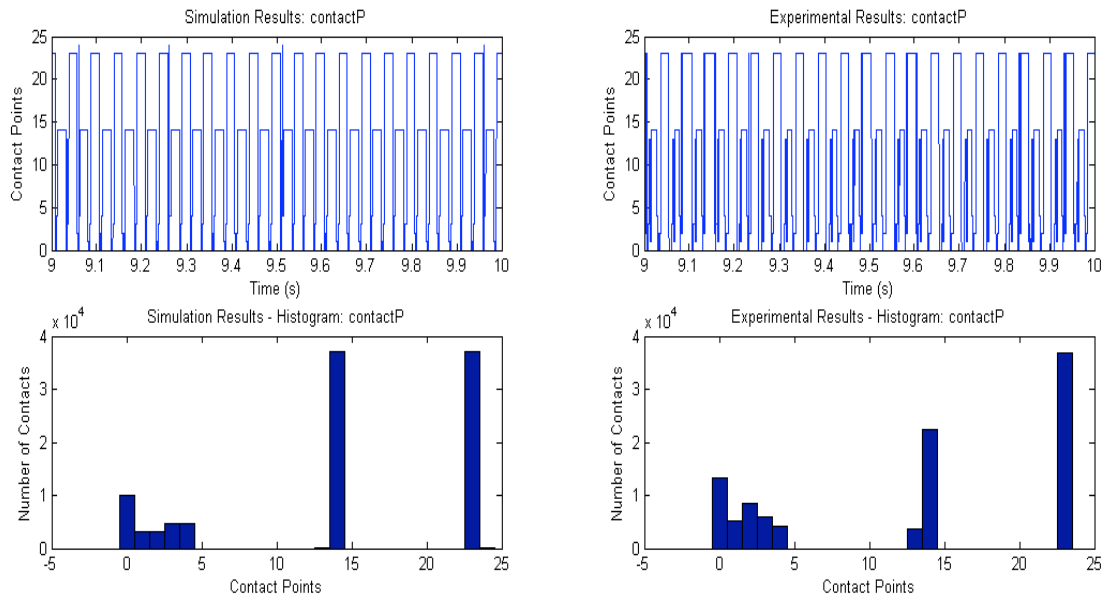


Figure 15 – Contact Time Histories and Histograms Results for Figure 10

Next, a sinusoidal sweep was conducted experimentally and simulated numerically. Again, the results were compared visually. Figure 16 shows the simulation and experimental results for the chirp from 5 Hz to 60 Hz over a four minute interval. The simulation managed to predict the main resonant frequency ranges, however, it seemed to die out much faster than the experimental results. A resonance jump at about 35 seconds seems to indicate a hardening nonlinearity in the experiment. In the simulation this jump may be at about 45 seconds, but there seems to be a softening type nonlinear jump resonance or the resonance may be washed out in the initial burst of the simulation. The smaller resonances after the large symmetric resonance near 150 seconds are indicated in both the experiment and the simulation.

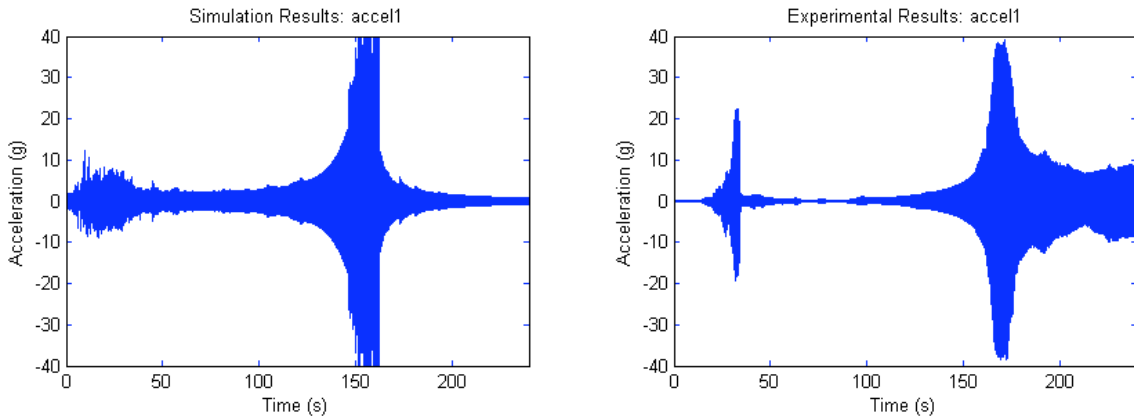


Figure 16 – Sine Chirp Results (Frequency Range: 5-60 Hz)

A wavelet analysis was conducted to compare the similarity of the signals at multiple resolutions. In Figure 17, the outcome of a wavelet decomposition of the experimental results is shown. The original signal measured from the first accelerometer is shown at the top of Figure 17. The various decomposition levels are shown below and to the left of the original signal in increasing order. The corresponding power spectrum of the FFT of each signal decomposition level is shown to the right. The same type of analysis for the simulation results for accelerometer 1 is shown in Figure 18. When comparing Figures 17 and 18, one can see the overall shape of each level is visually similar, although the amplitudes are different for some of them. The FFT results also compare and show the same type of correlation. The locations of the peaks are generally in the correct spot, but some of the amplitudes are different. The wavelet levels were computed using the 'db4' wavelet and 10 levels of decomposition (only the first five are shown). Levels 1, 2, and 3 match the shape of the signal very well, but the power spectrum amplitudes are wrong by an order of magnitude. Again, this may be from parameter mismatch, damping estimate errors, or nodal location of the accelerometers.

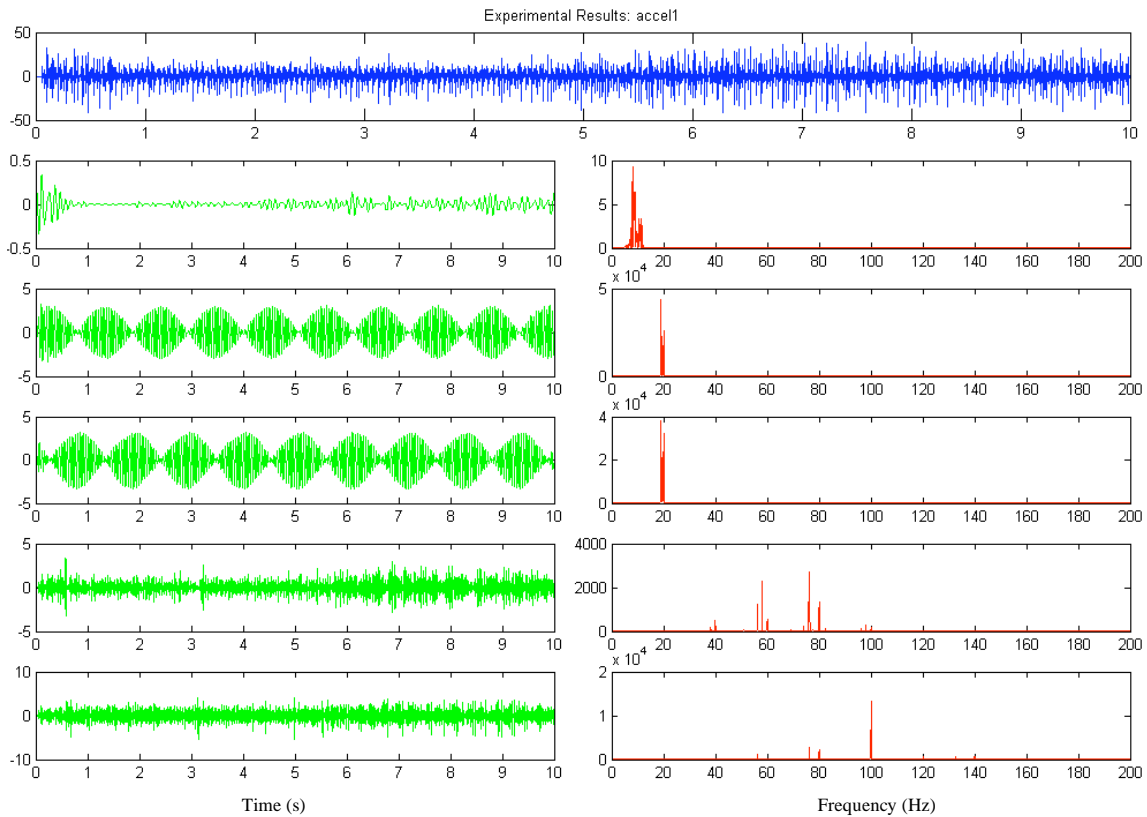


Figure 17 – Wavelet Analysis Accel 1 (Experiment): Wavelet Level (g), Power Spectrum

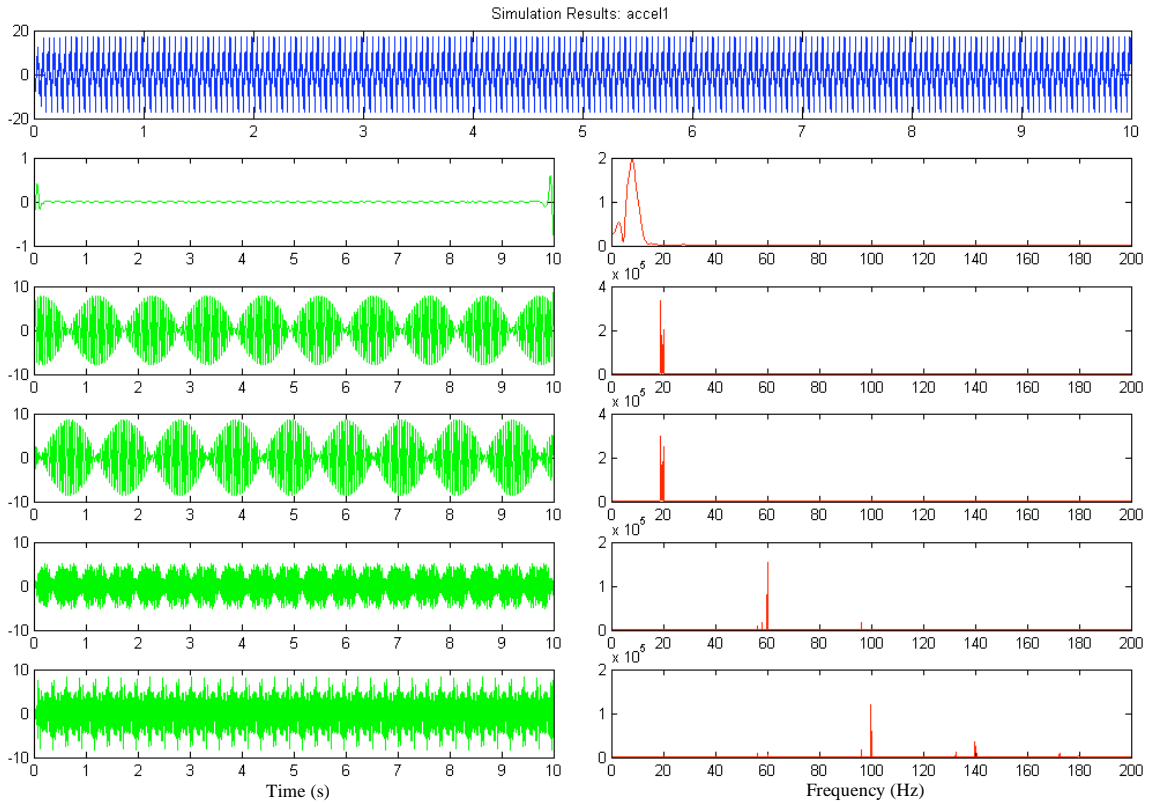


Figure 18 – Wavelet Analysis Accel 1 (Simulation): Wavelet Level (g), Power Spectrum

In order to better determine how the joint was moving, a high speed camera was used to capture the movement at 1000 frames per second. The results from the experiments were then compared to animations produced from the data output by the simulation. Figures 19 and 20 show the joint in a large displacement. The joint is rotated and the outer beam can be seen to be in contact at points 2 and 3, the same as in the video. Figures 21 and 22 show both the joint and the outer beam at the neutral axis.

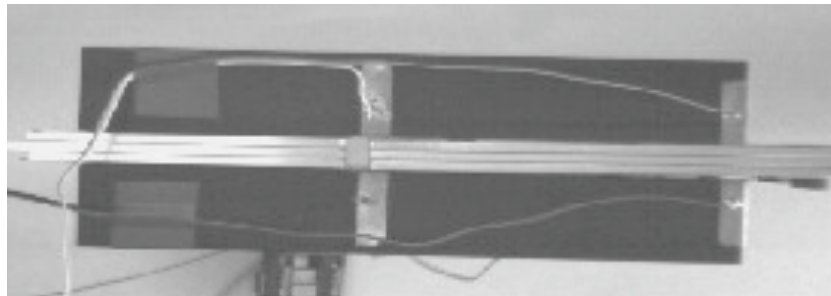


Figure 19 – Frame from High Speed Video, Displaced – Gap Width .0864cm

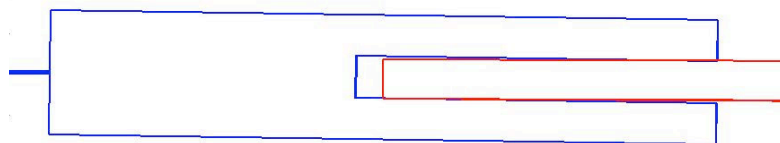


Figure 20 – Frame from Simulation Animation, Displaced – Gap Width .0864cm

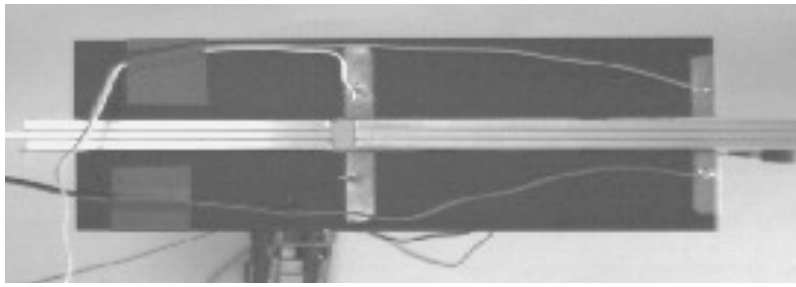


Figure 21 – Frame from High Speed Video, Neutral – Gap Width .0864cm

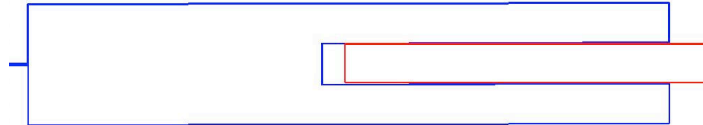


Figure 22 – Frame from Simulation Animation, Neutral – Gap Width .0864cm

The data was also looked at in the phase plane and using Poincare maps. Figure 23 is a phase plane map of the simulated tip deflection of the second beam. It shows the quasi-periodicity in the system. Figures 24 and 25 show a Poincare map of the same data at the 20Hz driving frequency. Figure 25 is zoomed in on one of the points which is actually a collection of points forming a line. This also shows that the simulation is predicting quasi-periodicity.

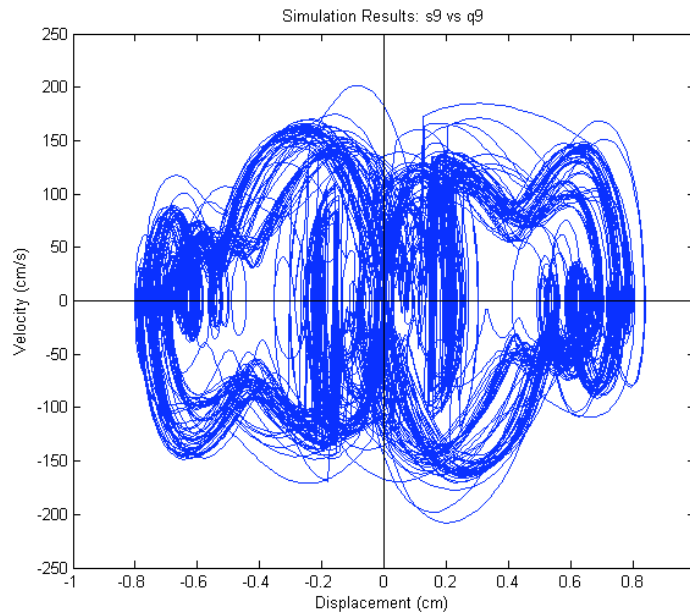


Figure 23 – Phase Plane Portrait of Tip Deflection

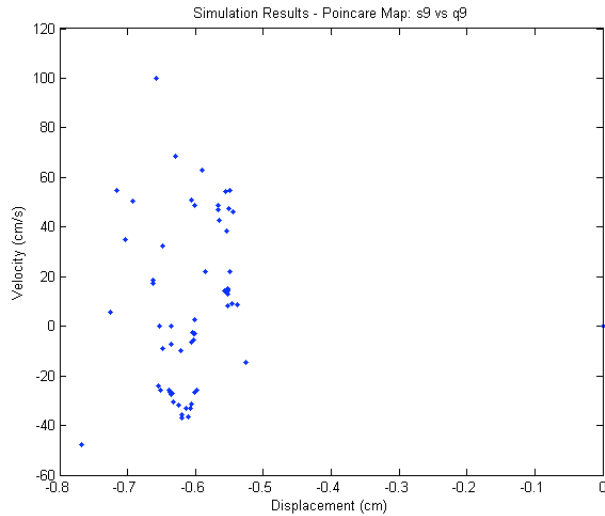


Figure 24 – Poincare Map of Tip Deflection

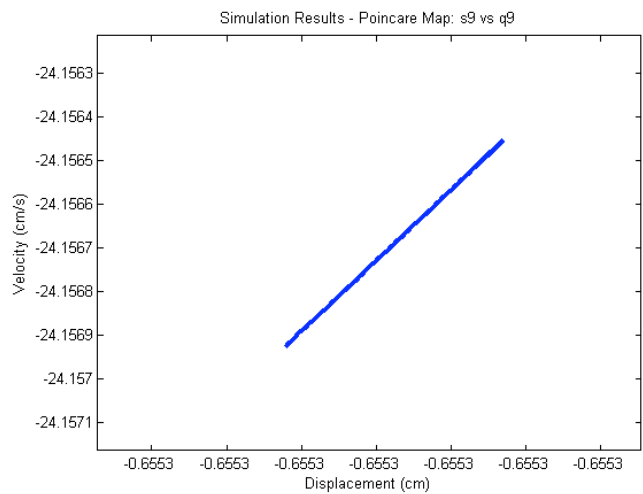


Figure 25 – Magnified Poincare Map of Tip Deflection

10 CONCLUSIONS

This project provides validation of a low order model of a highly nonlinear structure. The structure is a beam with a loose bolted joint. The looseness allows relative movement and impacts between the beam and the joint which cause complex nonlinearities. Many structures use bolted joints and it would be useful to be able to model their response caused by damage of this type.

The model was able to yield acceptable results when compared to the experiment in several areas. First, the model represented the impact nonlinearity well. The model was able to capture the impacts and transitions at each impact. This result is evident in how well the contact histories correspond. Second, the frequency content of the model matched very closely to the experiment. The strain also shows good matching of frequency content and amplitude. This is good evidence that the model captures the joint dynamics in the structure. The problem with the acceleration frequency content was that amplitudes of the frequencies were not matching very well between the model and the experiment. Possible reasons for this include the accelerometers being placed at nodes of the structure, parameter misidentification in the model, or a fundamental problem with the model. Accelerometer placement and improper parameter identification are thought to be the primary cause of the mentioned discrepancies. Third, the first five wavelet decomposition levels and the first three power spectrums of those levels displayed reasonable correspondence.

Even though the model displayed a few shortcomings, with some time and adjustment it could prove to be significantly useful. The level of detail captured by the model using only nine degrees of freedom illustrates the promise of the model. Compare this to the 7000 DOF used in the Pratt and Pardoen study [7]. Throughout testing of the structure, the model has displayed the ability to incorporate superharmonic events up to 600 Hz depending on the parameters used.

11 ACKNOWLEDGMENTS

Funding for this work via the Los Alamos Dynamics Summer School was provided by the Engineering Science and Applications Division at the Los Alamos National Laboratory and the Department of Energy's Critical Skills Programs Office. The following companies generously provided various software packages that were necessary to complete the student projects: Vibrant Technologies, ABAQUS Inc., The Mathworks. The fourth author also acknowledges the funding provided by the AFOSR (grant F49620-02-10083) for the initial theoretical modeling efforts of this work.

12 REFERENCES

- [1] A. A. Barhorst, An Elasto-Dynamic Model of a Slewing Beam with a Loose Bolted Lap Joint-Variable Structure Motion Model Development. To appear.
- [2] A. A. Barhorst, An Elasto-Dynamic Model of a Slewing Beam with a Loose Bolted Lap Joint-Momentum Transfer Model Development. To appear.
- [3] A. A. Barhorst, An Elasto-Dynamic Model of a Slewing Beam with a Loose Bolted Lap Joint-Simulation Algorithm and Results. To appear.
- [4] A. A. Barhorst, An Elasto-Dynamic Model of a Slewing Beam with a Loose Bolted Lap Joint-Experimental Results and Validation. To appear.
- [5] D.O. Smallwood, D.L. Gregory, R.G. Coleman, Damping Investigations of a Simplified Frictional Shear Joint, in: *Proceedings of 71st Shock and Vibration Symposium*, 2000.
- [6] C.J. Hartwigsen, Y. Song, D.M. McFarland, L.A. Bergman, A.F. Vakakis, Experimental Study of Non-linear Effects in a Typical Shear Lap Joint Configuration, *Journal of Sound and Vibration* 227 (2004) 327-351.
- [7] J. D. Pratt, G. Pardoen, Numerical Modeling of Bolted Lap Joint Behavior, *Journal of Aerospace Engineering*, (2002) 20-31.
- [8] C. W. Moloney , D. M. Peairs, E. R. Roldan, Characterization of Damping in Bolted Lap Joints, in: *Proceedings of International Modal Analysis Conference*, Kissimmee, FL, 2001.
- [9] A. A. Barhorst, Systematic Closed Form Modeling of Hybrid Parameter Multiple Body Systems, *The International Journal of Nonlinear Mechanics* 39(1), (2004) 63-78.
- [10] A. A. Barhorst, L. J. Everett, Modeling Hybrid Parameter Multiple Body Systems: A Different Approach, *The International Journal of Nonlinear Mechanics* 30(1) (1995) 1-21.
- [11] W.D. Iwan, On a Class of Models for the Yielding Behavior of Continuous and Composite Systems, *Journal of Applied Mechanics* 89 (1967) 612–617.
- [12] D.J. Segalman, An Initial Overview of Iwan Modeling for Mechanical Joints, Report SAND 2001-0811, Sandia National Laboratories, Albuquerque, NM, 2001.
- [13] D.W. Lobitz, D.L. Gregory, D.O. Smallwood, Comparison of Finite Element Predictions to Measurements from the Sandia Microslip Experiment, in: *Proceedings of International Modal Analysis Conference*, Orlando, FL, 2001.
- [14] L. Gaul, J. Lenz, Nonlinear dynamics of structures assembled by bolted joints, *Acta Mechanica* 125, (1997) 169-181.
- [15] J. Collins, M. Nothnagel, J. Pretko, A. Barhorst, Model Validation of Loose Bolted Joints in Damaged Structural Systems, in: *Proceedings of International Modal Analysis Conference*, Orlando, FL, 2005.